



Polyamide nanofilm composite membranes (NCMs) supported by chitosan-coated polyvinylidene fluoride (PVDF) nanofibrous mats and their separation properties

Guo-Rong Xu*, He-Li Zhao, Shui-Bo Wu

Institute of Seawater Desalination and Multipurpose Utilization (Tianjin), State Oceanic Administration (SOA), Tianjin 300192, China, Tel. +86 022 87896336; emails: labxgr@aliyun.com (G.-R. Xu), 17847102@qq.com (H.-L. Zhao), 317377322@qq.com (S.-B. Wu)

Received 20 April 2015; Accepted 17 December 2015

ABSTRACT

Desalination provides an effective method to solve the problem of freshwater shortage, which is currently the most urgent issue around the world. Among all the desalination methods, membrane desalination is superior to others due to its unique advantages, such as easy operations and high separation performance. Specially, polyamide thin-film composite (PA-TFC) reverse osmosis membranes are the dominant desalination membranes in recent decades and have been widely used all around the world. However, the comparatively high operating pressures and low water permeations make them non cost-effective and have seriously restricted their wider applications. Electrospun nanofibrous membranes (ENMs) have shown great promising applications in the filtration areas. ENMs-based filtration membranes can provide higher permeations under the same operating conditions. Therefore, in the current work, a novel PA-TFC membrane supported by ENMs is designed. The ENMs-supported PA-TFC membranes show apparently high water flux ($2.06 \text{ L m}^{-2} \text{ h}^{-1} \text{ bar}^{-1}$) with a salt rejection of 94.4%. More importantly, the operating pressure is only 8 bar, which is lower than most of the currently used and researched PA-TFC membranes. The fabricated membranes are more cost-effective and can be used in some unique desalination areas which need as high as permeations and moderate salt rejections.

Keywords: Reverse osmosis; Nanofibrous membranes; Electrospinning; Coating layer; Polyamide membrane

1. Introduction

Currently, population growth and enhanced living standards, together with the expansion of industrial and agricultural activities, are creating unprecedented demands on clean water supplies all over the world [1,2]. It is evaluated that 3.9 billion people in 52

countries will suffer from water shortage by year 2025, and that by year 2030, the global needs of water will increase to 6,900 billion m^3 from the current 4,500 billion m^3 [3]. It has become one of the most imperative issues for the worldwide people to solve the problem of water shortage. Given the fact that only 0.5% of the total water resource on earth is potable, fresh water, while 97% is seawater, desalination which could convert seawater into fresh water provides a

*Corresponding author.

solution to meet the increasing water consumption [1]. Therefore, researchers have developed many effective desalination technologies, which are categorized into thermal-based processes (e.g. multi-stage flash (MSF), multiple-effect distillation (MED) and vapor compression distillation (VCD)) and membrane-based separation processes (e.g. electrodialysis (ED), nanofiltration (NF), and reverse osmosis (RO)) [4]. Membrane-based separation processes are superior to thermal-based processes due to their cost-effectiveness, versatility, and easy operation properties. Particularly, RO has developed rapidly over the last decades into the dominant technology for water desalination [5]. Most RO membranes are based on cellulose acetate (CA) and aromatic polyamides (PAs) [6]. However, PAs-based thin-film composite (PA-TFC) membranes have overwhelmingly dominated the RO membranes desalination due to their superior properties to CA-based membranes, such as superior water flux, salt and organics rejections, pressure compaction resistance, wider operating pH range (1–11), and temperature range (0–34°C), and higher stability to biological attack, despite its comparatively low chlorine tolerance [4,6].

Biofouling and chlorination are the two key problems that inhibit the optimized applications of PA-TFC RO membranes [7,8]. Many strategies, including surface modifications [9–14], surface coating [15–19], and incorporation of inorganic nanoparticles in the active layer [20–25], have been developed to improve the fouling/chlorine resistance of the PA-TFC RO membranes. All these methods are designed to alter the properties of surface active layer. Nevertheless, the sublayers, which are characterized by pore sizes, mass transfer resistance, and hydrophilicity, can also play important roles on the structures and separation properties of PA-TFC RO membranes [7]. The sublayers providing support for the barrier layer should be biologically, mechanically, chemically, and thermally stable. And their structures and physical and chemical properties can influence the formation of the barrier layers [26]. For example, Ghosh et al. prepared a kind of compaction-resistant PA-TFC RO membrane by polymerizing polyamide film on porous polymeric support with micro- and/or nanoparticles dispersed therein [27]. Dispersion of micro- and/or nanoparticles in the polymeric sublayer can effectively reduce “internal fouling” which is characterized by a flux decline over time, especially at the initial stage of the desalination process. The obtained compaction resistant membrane exhibited a flux decline of 10–50% less than that prepared on the polymeric sublayer without micro- and/or nanoparticles dispersion. Thus, it is possible to adjust the structures and separation

properties of PA-TFC RO membranes by altering the sublayers.

Various excellent properties, such as high Brunauer–Emmett–Teller (BET) surface areas (9–51 m²/g), small and tunable fibers diameters (5–50 nm), small pore sizes (2.7–0.17 μm), and high porosities (20–80%), make electrospun nanofibrous membranes (ENMs) promising materials for the liquid separation applications [28]. Actually, ENMs have proved to be good candidates for water treatment and have been extensively used in membrane-based separation technologies. ENMs can be directly used as microfiltration membranes [29]. When being used in ultrafiltration [30], especially nanofiltration [31], ENMs were always used as the sublayers with further modifications. ENMs exhibit evident advantages when being used as the sublayers. For example, compared with commercial ones, ENMs-based PA-TFC nanofiltration membranes exhibited distinctly higher permeate flux while maintaining rejection rate, which was due to the creation of “water-channel” in the unique interfacial region between the nanofibers and the ultrathin barrier layer [31]. Moreover, ENMs-supported composite membranes prepared via interfacial polymerization have shown some potential on NaCl rejections [32]. However, piperazine (PIP) was mostly used as aqueous phase rather than *m*-phenylene diamine (MPD), which was more commonly used. This motivates us to further investigate the desalination properties of ENMs-supported PA-TFC RO membranes prepared using MPD as the aqueous phase.

In our previous work, we have investigated the practicability of fabrication of polyamide nanofilm composite membranes (NCMs) with potential applications for desalination by interfacial polymerization of MPD and TMC despite the low salt rejections [33]. Herein, we reported new NCMs supported by Poly(vinylidene fluoride) (PVDF) nanofibrous membranes. Under the optimized conditions with MPD concentration of 2.5 wt%, TMC concentration of 0.125 wt%, and curing time of 15 min at temperature of 75°C here, the PVDF-based NCMs (PVDF-NCMs) show apparently high water flux (2.06 L m⁻² h⁻¹ bar⁻¹) with a salt rejection of 94.4%.

2. Experimental

2.1. Materials and reagents

Poly(vinylidene fluoride) (PVDF) was purchased from Yangyun Plastic Mater Co., Ltd. Chitosan with the degree of deacetylation (DD) of 80.0–95.0 and a viscosity of 50–800 mPa s was purchased from Sino-pharm Chemical Reagent Co., Ltd. Glutaraldehyde

(A.R., 50%) and n-hexane (A.R., $\geq 95.0\%$) were purchased from Tianjin Fuchen Chemical Works. M-phenylenediamine (MPD, A.R., $\geq 99\%$) was purchased from Tianjin Guangfu Fine Chemical Research Institute. 1,3,5-Benzenetricarbonyl trichloride (TMC) was purchased from Aladdin Chemistry Co., Ltd. Sodium hydroxyl (NaOH, A.R., $\geq 96.0\%$), sodium chloride (NaCl, A.R., $\geq 99.5\%$), acetic acid (H_3COOH , A.R., $\geq 99.5\%$), sodium lauryl sulfate (SLS), and N,N-dimethylformamide (DMF, A.R., $\geq 99.5\%$) were all purchased from Beijing Chemical Works. All the materials and reagents were used as received without any purification.

2.2. Preparation of PVDF-NCMs

The preparation process of PVDF-NCMs involves three procedures: (1) preparation of PVDF nanofibrous membranes by electrospinning on the supporting layer (non-woven fabric); (2) coating of chitosan layer on the surface of electrospun PVDF nanofibrous membranes; and (3) interfacial polymerization (IP) on the surface of chitosan-coated electrospun PVDF nanofibrous membrane to form NCMs.

The structure difference between the obtained PVDF-NCMs and traditional PA-TFC membranes is shown in Fig. 1(a). SEM images for PVDF nanofibrous membrane before and after chitosan coating are shown in Fig. 1(b) and (c) and Fig. 1(d) shows the fiber diameter distributions. The PVDF nanofibers exhibit continuous and smooth surface morphology with the average diameter (AFD) of 30 nm and standard deviation (SD) of 117 nm. After the chitosan coating, the nanofibrous membrane is covered with a very thin chitosan layer. As is depicted in our previous research, the chitosan coating solution can effectively impregnate the PAN nanofibers network and fill the pores of network, which will compensate the defects introduced by the pores existing in the nanofibrous mats and inhibit the formation of pinhole defects in the resulting membranes [33]. Fig. 2(c) and (d) shows the water flux of PVDF nanofibrous membranes before and after chitosan coating. Chitosan coating dramatically decreases the water flux from 460 to 280 $\text{L}/\text{m}^2 \text{ h}$.

2.2.1. Electrospinning of PVDF

4.75 g of PVDF was dissolved in 20 ml of N,N-dimethylformamide (DMF) and stirred under magnetic condition for one day to form a homogeneous solution. PVDF nanofibrous mats were prepared by electrospinning. The electrospinning was carried out on a typical electrospinning apparatus at room tem-

perature. The solution was supplied at a rate of 1.5 ml h^{-1} and the positive voltage applied on the needle was 18 kV. A roller with a rolling speed of 70 rpm was used as the collector and the distance between the collector and the needle was 25 cm. Under this condition, the well uniform ENMs can be obtained.

2.2.2. Synthesis of chitosan-coated PVDF nanofibrous membrane

1.00 g of chitosan was dissolved in 200 ml of $\text{H}_2\text{O}/\text{CH}_3\text{COOH}$ (99/01, v/v) mixed solution and stirred under the magnetic condition for 5 h to form a homogeneous solution. Then, 2 ml of glutaraldehyde (GA) was added into the solution and stirred for 20 min. The PVDF nanofibrous membrane was immersed into the chitosan solution for 30 min and then the coating process was carried out on a spin coater. After the coating, the coated membrane was kept airproof for 12 h to facilitate the chitosan cross-linking which resulted in the formation of a thin-film layer on the surface of PVDF nanofibrous membrane. Finally, the coated membrane was stored in DI water for use.

2.2.3. Interfacial polymerization

MPD aqueous solution with a concentration of 2.0% (w/v) including 0.15% (w/v) of SLS and TMC n-hexane solution with a concentration of 0.1% (w/v) were first prepared. After stirring for 1 h, MPD aqueous solution was purged into the organic glass frame which fixed the chitosan-coated PVDF nanofibrous membrane and the immersion was kept for at 30 min. The excess MPD droplets on the membrane surface were removed by rolling a rubber roller firmly across the membrane surface. Then, the TMC n-hexane solution was poured into the frame to begin the interfacial polymerization (IP) reaction for 90 s to form PVDF-NCMs. The obtained membranes were then dried at room temperature for 10 min and then cured at the temperature of 75°C for 15 min. Finally, the membranes were washed with DI water and stored in DI water at the temperature of 5°C for use.

2.3. Characterizations of PVDF-NCMs

Scanning electron microscopy (SEM) images were collected on a field emission SEM (FESEM, S-4800, Hitachi, Japan). The diameter distribution and the average fiber diameter (AFD) were calculated by a custom code image analysis program (SMile View). Atomic force microscopy (AFM) images were obtained by a Dimension 3100 AFM, operating in tapping mode

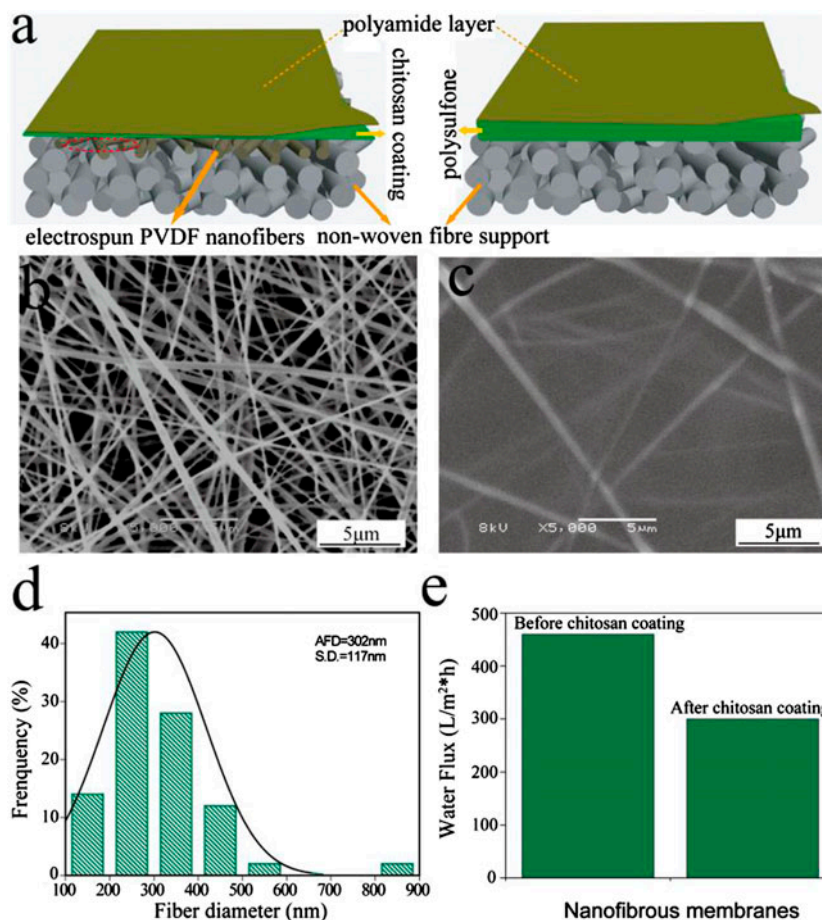


Fig. 1. (a) Structural comparison between the obtained PVDF-NCMs supported by chitosan-coated ENMs and traditional PA-TFC membranes supported by polysulfone layer, (b and c) SEM images for PVDF nanofibrous membranes before and after chitosan coating, (d) fiber diameter distributions of PVDF nanofibrous membranes, and (e) water flux of PVDF nanofibrous membranes before and after chitosan coating.

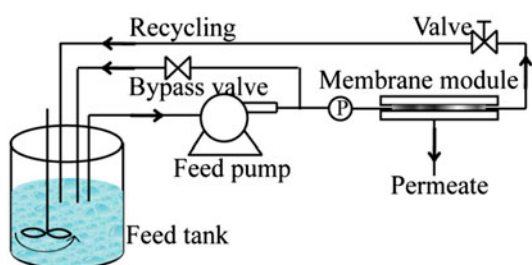


Fig. 2. The lab-scale cross-flow filtration rig used for the performance test of the obtained RO membranes.

with a scan rate of 1.20 Hz and a resolution of 256×256 . An n-doped silicon tip with 1–10 Ω cm phosphorus (Veeco, MPP-11100-140) was used as the probe. Contact angles (CA) of the samples were measured using sessile drop method on a Contact

Angle System (Dataphysics, Germany). The samples were dried sufficiently before the measurement. Then, the measurement was performed as follows. A dangling droplet of 1 μ L of deionized water was carefully deposited on the samples surface for certain times, and the CA was recorded by the accompanied software. Each sample measurement was carried out for at least 10 times at different locations and the CA was obtained from the average values.

2.4. Desalination properties evaluation

Desalination properties of the obtained PVDF-NCMs in terms of permeations and salt rejections were investigated by employing lab-scale cross-flow filtration rig (Fig. 2) using artificial brackish water with a composition of 1,000 mg/L of NaCl. Before the tests, the membranes were first pressed at a lower

pressure of 0.5 MPa (5 bar or 75 Psi) for 0.5 h. Then, the pressure was adjusted to 0.8 MPa (8 bar or 120Psi) and permeates flux and salt rejections were measured at the time intervals of 30 min. Permeates were calculated by collecting the volume of the permeate solution through the membrane in a given time period,

and salt rejections were evaluated by the concentration of the NaCl in the feed and permeate solution:

$$J_w = \frac{\Delta V}{A \times \Delta t} \quad (1)$$

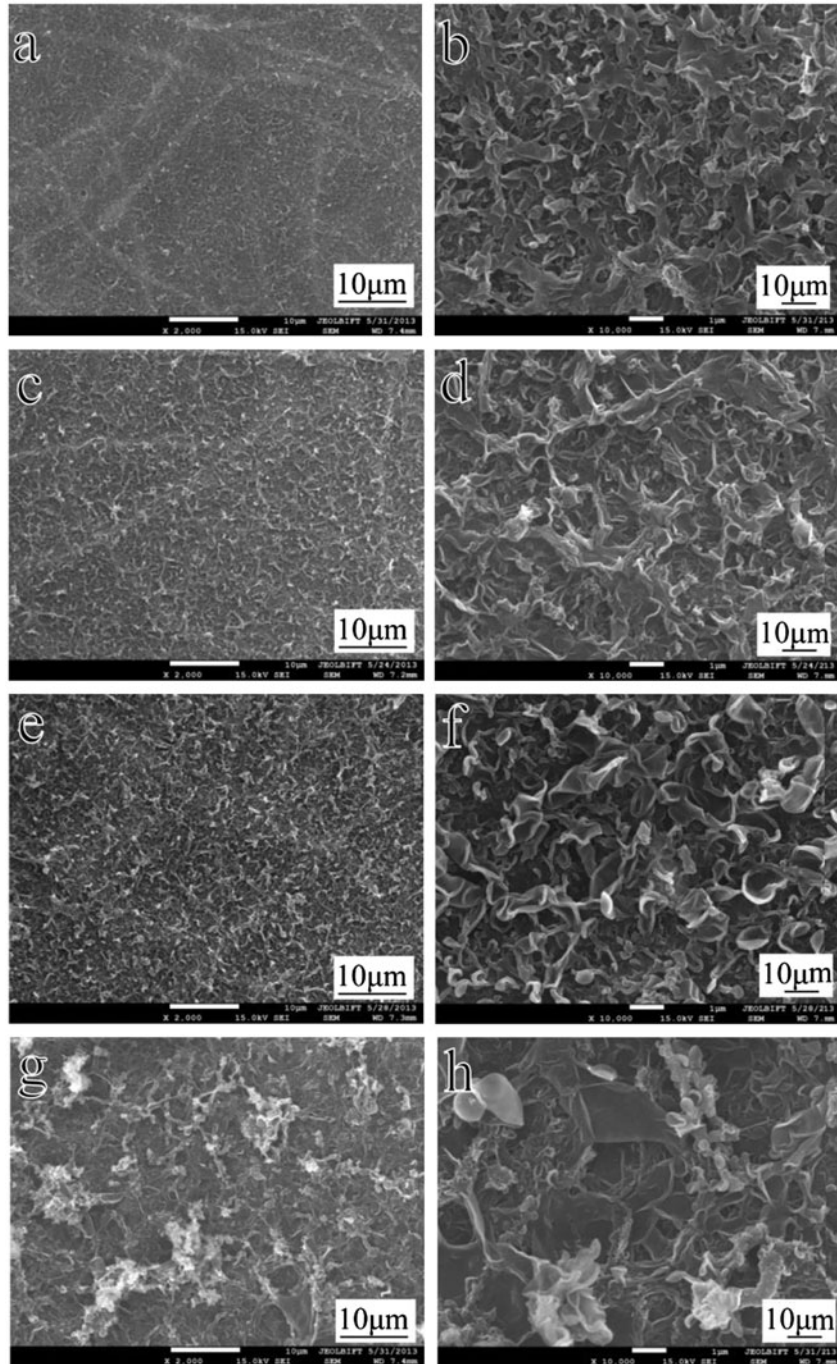


Fig. 3. Low and high magnified SEM images for the obtained PVDF-NCMs with different MPD concentrations (a and b) 1.5 wt%, (c and d) 2.0 wt%, (e and f) 2.5 wt%, and (g and h) 3.0 wt%. (TMC concentration is 0.150 wt%).

$$R(\%) = \left(1 - \frac{C_p}{C_f}\right) \times 100 \quad (2)$$

where J_w (L/m² h) is the permeate flux, A (m²) is the effective membrane area, ΔV (L) is the volume of the permeate solution collected during a time period Δt (h), R is the apparent salt rejection, C_f and C_p (mg/L) are the concentration of the NaCl in the feed permeate solution, respectively. C_f and C_p are calculated according to the conductivity of the solution measured using a conductivity meter (DDS-11A, Changzhou Maikenuo Instrument Co., Ltd).

3. Results and discussions

3.1. Influence of MPD concentrations

Defect free PA-TFC membranes are all obtained with MPD concentrations in the range from 1.5 to 3.0 wt%. Increasing MPD concentrations leads to the thicker barrier layer, which can be seen from low-magnified SEM images in Fig. 3(a), (c), and (e). When the MPD concentration is 1.5 wt%, the supporting nanofibers can be seen distinctly (Fig. 3(a)). When MPD concentration is increased to 2.0 and 2.5 wt%, it seems that the supporting nanofibers are better covered by the barrier layer (Fig. 3(c) and (e)). High-magnified SEM images in Fig. 3(b), (d), and (f) give more detailed information for the influence of MPD concentrations on the membranes morphologies. The membranes obtained with MPD concentration of 1.5 and 2.0 wt% show peak-and-valley structures, which might be caused by the roughness of supporting layer. When MPD concentration is increased to 2.5 wt%, peak-and-valley structures transform into nanosheets with high density and it seems that the barrier layer entirely covers the supporting nanofibrous mats. Further increase in MPD concentration to 3.0 wt% leads to agglomeration (Fig. 3(g) and (h)), which is ascribed to the accumulation of MPD in the amino end group. It has been reported that for the fixed TMC concentration, there exist a threshold for the MPD concentration [34]. Below the threshold, increase in MPD concentration will increase the thickness of the barrier layer until the formation of the maximum thickness. And further increasing MPD concentrations above the threshold will increase the density of the active layer, and the thickness will remain unchanged [34]. Combined with SEM images in Fig. 3, it is concluded that the threshold herein for the TMC concentration of 0.150 wt% is 2.5 wt%.

The correlations between the MPD concentrations and the hydrophilicity of the obtained membranes are

shown in Fig. 4. Under each fixed contacting time, the contact angles of the membranes obviously increase with increasing MPD concentrations. For instance, the contact angles of the membranes with MPD concentration of 1.5, 2.0, 2.5, and 3.0 wt% are 94, 123.8, 136.3, and 137.8°, respectively with contacting time of 60 s. However, for all membranes the contact angles decrease gradually with increasing contacting times until the droplets thoroughly spread across the membranes surfaces, which is reflected by the contact angle of 0°. But the time needed for the complete spread increases apparently with increasing MPD

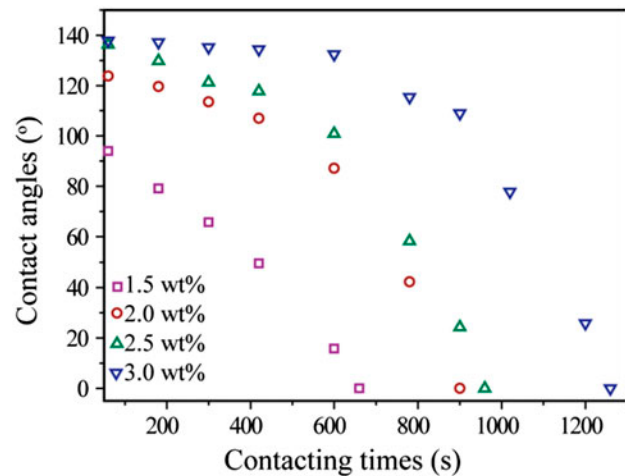


Fig. 4. Correlations between the contact angles and contacting times for the PVDF-NCMs obtained with different MPD concentrations.

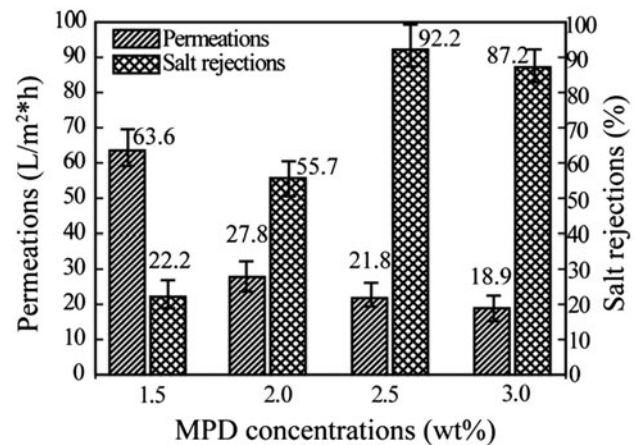


Fig. 5. Influence of MPD concentrations on the separation performance of the PVDF-NCMs in terms of permeations and salt rejections (experimental conditions: 2,000 ppm NaCl aqueous solution as the feed; pressure: 0.8 MPa; 25°C).

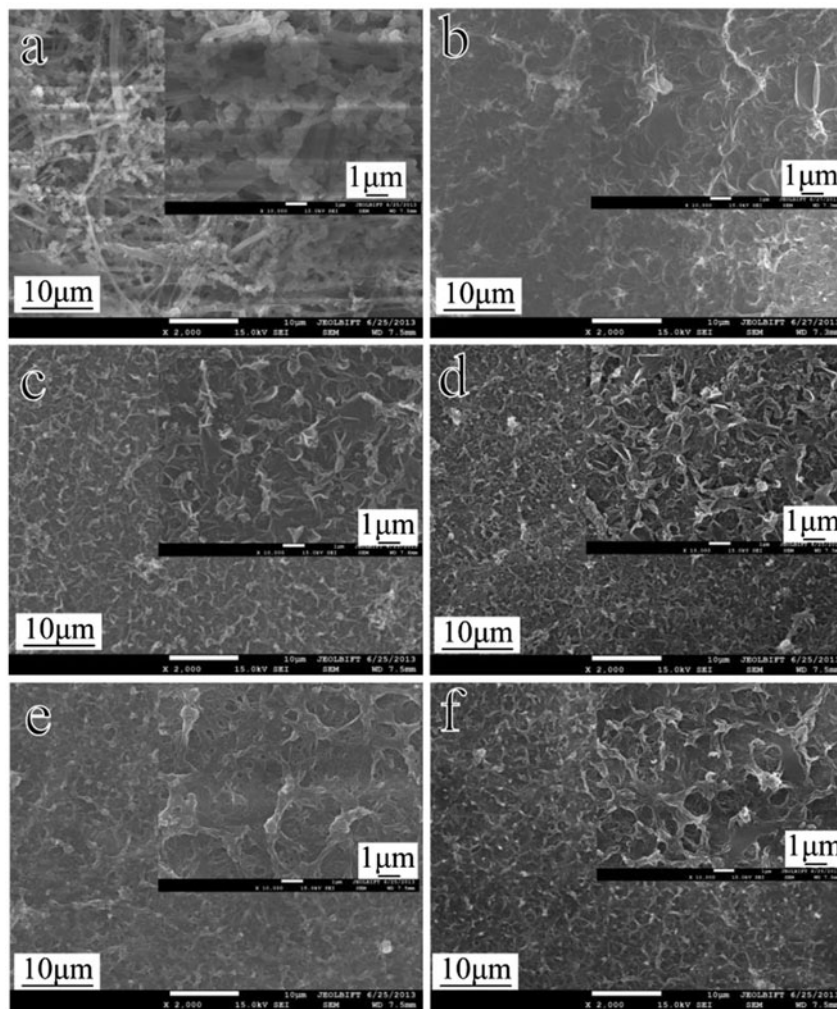


Fig. 6. SEM images for the obtained PVDF-NCMs with different TMC concentrations (a) 0.075 wt%, (b) 0.125 wt%, (c) 0.150 wt%, (d) 0.227 wt%, (e) 0.303 wt%, and (f) 0.380 wt% (MPD concentration is 2.5 wt%, the inset shows the high magnified images).

concentrations. As shown in Fig. 4, for the membranes obtained with MPD concentrations of 1.5, 2.0, 2.5, and 3.0 wt%, the times needed for the total spread of droplets are 660, 900, 960, and 1,260 s, respectively. Moreover, it can be noticed that the contact angle of the membrane with MPD concentration of 1.5 wt% gradually decreases from 94° to 0° with increasing contacting times. However, the contact angles of the membranes with MPD concentration of 2.0, 2.5, and 3.0 wt% decrease very slowly in the initial stage, and then decrease to 0° more sharply compared with that of 1.5 wt%.

The membrane surface hydrophilicity is in close relation to the surface roughness. Usually, a rougher surface always exhibits a lower hydrophilicity, which is indicated by a larger contact angle. When the MPD

concentration is 1.5 wt%, the comparatively loose polyamide layer lets the droplet gradually spread across the membrane surface, thus the contact angle gradually decreases as the contact times increase. For the membranes with the MPD concentrations of 2.0, 2.5, and 3.0 wt%, the larger contact angles in the initial stage are ascribed to the rougher surface, which can be obviously observed by the high-magnified SEM images in Fig. 3. After conquering the resistance of roughness, the contact angles decreased sharply in the similar trend as that of 1.5 wt% (Fig. 4), because at this stage they own the same polyamide structure.

The influence of MPD concentrations on the surface structures and hydrophilicity of the PVDF-NCMs will definitely further affect their separation properties, as shown in Fig. 5. The permeations decrease

obviously while the salt rejections increase oppositely with increasing MPD concentrations in the range of 1.5 to 2.5 wt%. When MPD concentration is increased from 1.5 to 2.0 wt%, the permeation dramatically decreases from 63.6 to 27.8 L/m² × h, and further increase in MPD concentration leads to further slight decrease (21.8 L/m² × h). However, the salt rejections gradually increase from 22.2 to 92.2%. The decreased permeations and increased salt rejections are caused by the increased thickness and enhanced cross-linking degree of the barrier layer, as observed by the SEM images in Fig. 3. When the TMC concentration is fixed, the degree of cross-linking of the polyamide layer is first increased till the optimized MPD/TMC concentration ratio (ca. 20, w/w) reaches. Further increase in the MPD concentrations will decrease the degree of the cross-linking because it favors the formation of polyamide with smaller molecular weight [34]. When the MPD concentration is further increased to 3.0 wt%, although the permeation is further decreased to 18.9 L/m² × h, the salt rejection is not further increased. The decreased permeation was ascribed to the increased density of the surface polyamide layer, as is depicted in Fig. 3. And the decreased salt rejection can be explained by the “dilution effect.” As “dilution effect” indicates, the reduced water flux can reduce the dilution of the salt flux, thus decrease the salt rejections. Therefore, the optimized MPD concentration is fixed at 2.5 wt%.

3.2. Influence of TMC concentrations

The effect of TMC concentrations on the surface structures of the obtained PVDF-NCMs are shown in Fig. 6. When the TMC concentration is 0.075 wt%, the polyamide barrier layer cannot be formed on the surface of chitosan-coated ENMs (Fig. 6(a)). The inset high-magnified image indicates that only some aggregates are obtained. For the TMC concentrations of 0.125, 0.150, 0.227, 0.303, and 0.380 wt%, membranes with good barrier layer can be obtained (Fig. 6(b)–(f)). The surface morphology changes with increasing TMC concentrations can be observed by the inset high magnified images in each figure. Below the concentration of 0.227 wt%, the density of the nanosheets constituting the surface structure of the membranes increases with increasing TMC concentrations. The surface structure changes dramatically when the TMC concentration is higher than 0.227 wt% (0.303 and 0.380 wt%), nanosheets disappear and peak-and-valley structure with serious aggregation appears. The aggregation is supposed to be induced by the excessive TMC during the interfacial polymerization. The residual acyl chloride groups of TMC after the interfacial poly-

merization can hydrolyze into carboxylic groups on the membrane surface, which could induce aggregation by hydrogen bonding effect.

The contact angles with different contacting times for the PVDF-NCMs obtained with various TMC concentrations are shown in Fig. 7. The change in the contact angles can be divided into two stages. The contact angles decrease significantly when the TMC concentration increases from 0.125 to 0.150 wt%, and then change slightly when the TMC concentration further increases to 0.227 and 0.303 wt%. However, when TMC concentration increases to 0.380 wt%, the contact angles further decrease significantly. The decrease in the contact angles in the first stage is supposed to be mainly induced by the increase in the nanosheets density, which can be observed from the SEM images in Fig. 6. The increased nanosheets density can increase the surface roughness, which can further increase the hydrophilicity characterized by decreased contact angles. The further decrease in the contact angles in the second stage is dominantly ascribed to the excess TMC. When the TMC concentration is 0.380 wt%, which is far higher than that needed for the interfacial polymerization, more residual acyl groups are formed on membrane surface due to the lower cross-linking degree and thereby more carboxylic groups are produced via hydrolyzation. The hydrophilic carboxylic groups can significantly decrease the contact angles of the membranes.

The effect of the TMC concentrations on the separation properties of the obtained PVDF-NCMs are shown in Fig. 8. Obviously, the permeations gradually increase and the salt rejections gradually decrease with increasing TMC concentrations. Generally, the permeations and salt rejections are in close relation to

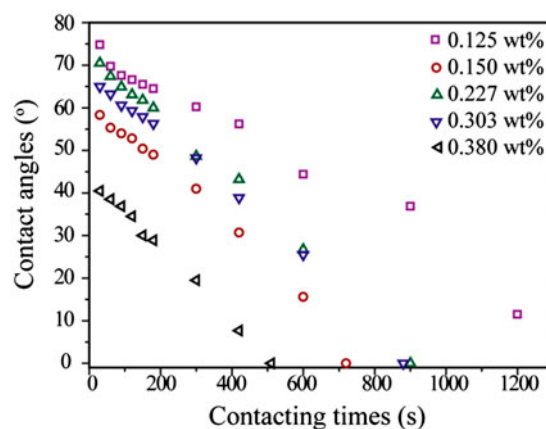


Fig. 7. Correlations between the contact angles and contacting times for the PVDF-NCMs obtained with different TMC concentrations.

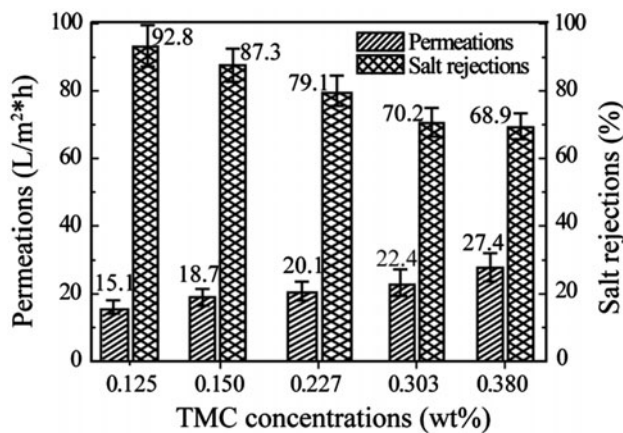


Fig. 8. Influence of TMC concentrations on the separation performance of the PVDF-NCMs in terms of permeations and salt rejections (experimental conditions: 2,000 ppm NaCl aqueous solution as the feed; pressure: 0.8 MPa; 25 °C).

the cross-linking degree of the polyamide layer. As mentioned above, when the MPD concentration is fixed, the cross-linking degree of the polyamide layer first increases till the optimized MPD/TMC concentration ratio (ca. 20, w/w) reaches. Further increase in the TMC concentrations will decrease the cross-linking degree [34]. It should be noted that not like the conventional polysulfone-supported polyamide RO membranes, when the TMC concentration is lower than 0.125 wt%, the low cross-linking makes it unable to form the polyamide layer on the composite electrospun nanofibrous PVDF support, as shown in

Fig. 6(a). Thus, the first used TMC concentration (0.125 wt%) in the separation properties measurements is the optimized one. Likewise, further increasing the TMC concentrations will decrease the cross-linking degree of the polyamide layer and induce the increased permeations and decreased salt rejections.

3.3. Influence of curing times

In the preparation of PA-TFC RO membranes, curing is always required after the interfacial polymerization to remove the residual organic solvents and to promote the additional cross-linking. Curing time and curing temperature have similar effect on the properties of the membranes. Prolonging the curing time or increasing the curing temperature will first increase the permeations due to the complete evaporation of the organic solvents. But at the same time, curing will also result in additional cross-linking of polyamide layer and shrinkage of support membranes pores, which will decrease the permeations but increase the salt rejections [35]. Therefore, it is of great importance to investigate the effect of the curing conditions on the morphologies and separation properties of the obtained membranes.

Curing time is selected to investigate the effect of curing conditions on the morphologies and separation properties of the obtained PVDF-NCMs. The SEM images of the membranes obtained with different curing times at the temperature of 75 °C are shown in Fig. 9. When the curing time is 5 min, the surface

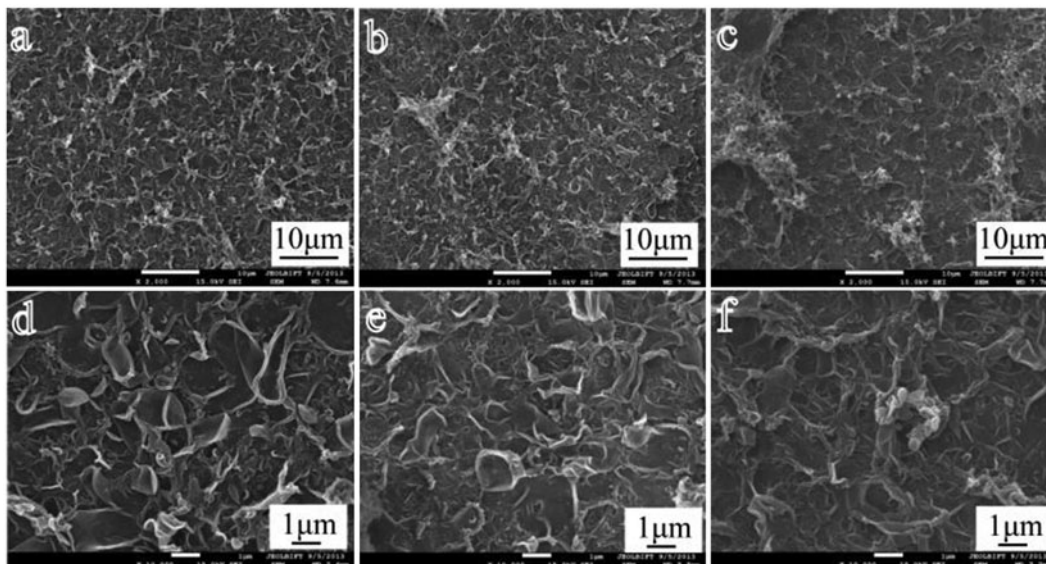


Fig. 9. Low and high magnified SEM images for the obtained PVDF-NCMs with different curing times (a and d) 5 min, (b and e) 15 min, and (c and f) 25 min (the curing temperature is 75 °C).

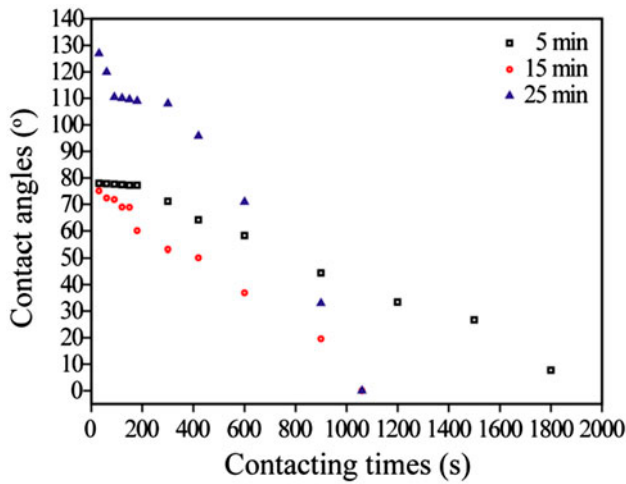


Fig. 10. Contact angles for the obtained PVDF-NCMs with different curing times (the curing temperature is 75°C).

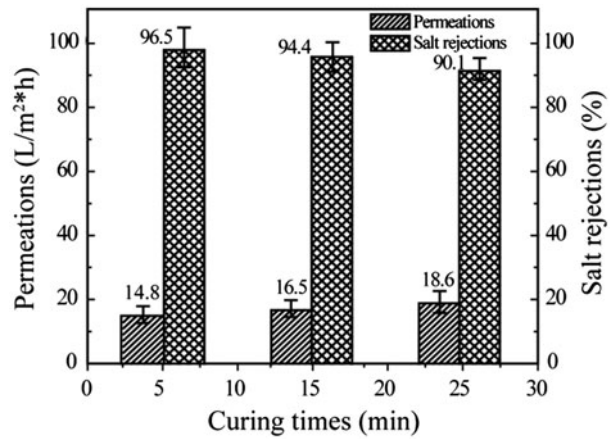


Fig. 11. Effect of curing times on the obtained PVDF-NCMs (the curing temperature is 75°C).

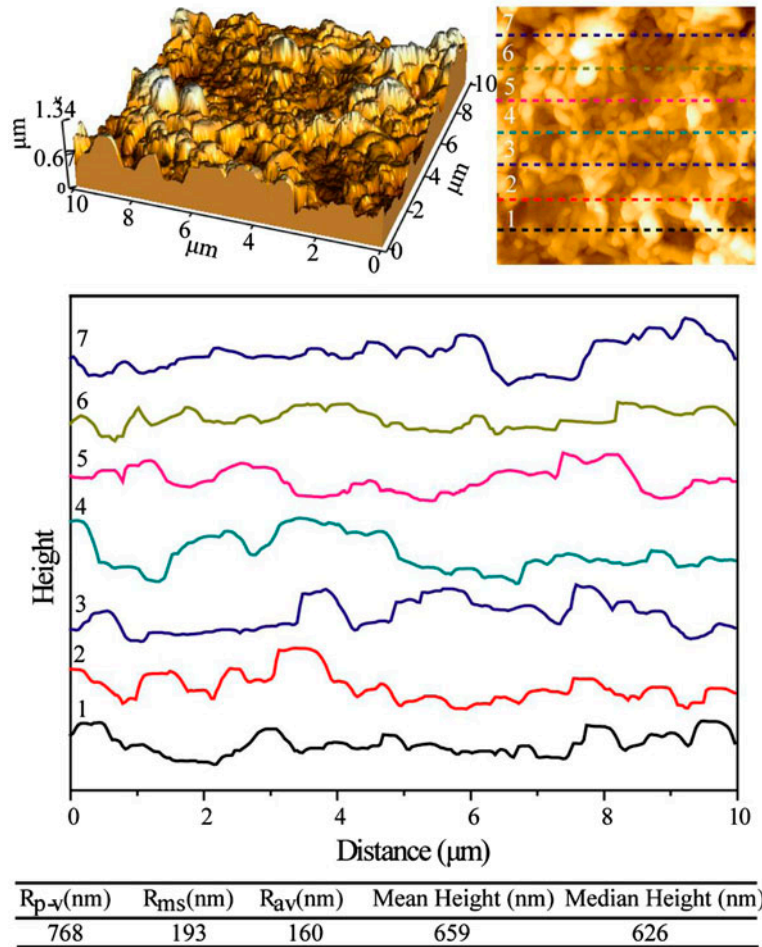


Fig. 12. AFM analysis for the PVDF-NCMs obtained with optimized condition.

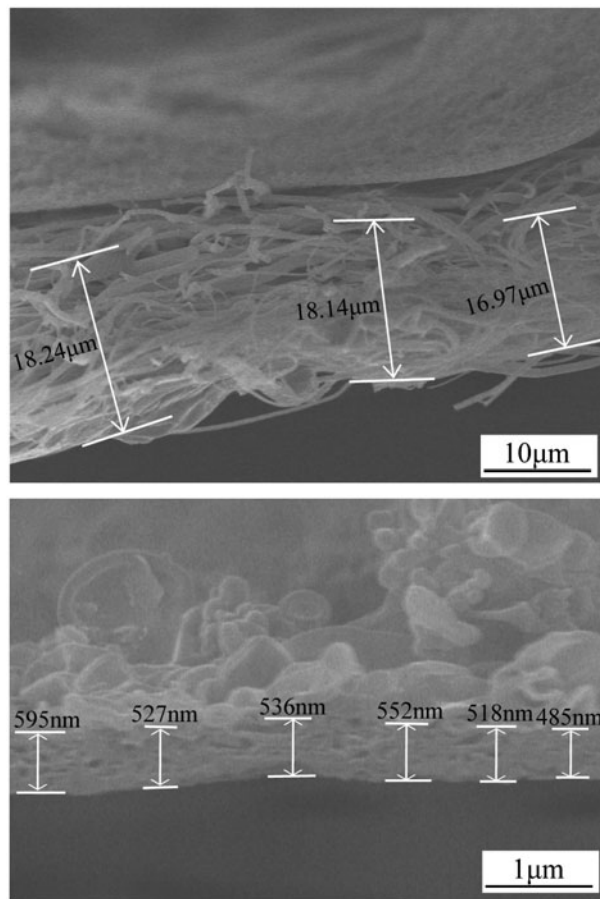


Fig. 13. Cross-sectional SEM images for the obtained PVDF-NCMs with optimized preparation conditions.

structure of the membrane consists of nanosheets with high density (Fig. 9(a) and (d)). The membrane with curing time of 15 min shows the similar surface morphology with that of 5 min, but the density of nanosheets seems to decrease (Fig. 9(b) and (e)). When the curing time is prolonged to 25 min, dramatic change occurs. First, severe aggregations can be found (Fig. 9(c)). In addition, the surface morphology transforms from nanosheets to peak-and-valley structure (Fig. 9(f)). The effect of the curing on the morphologies of the PVDF-NCMs supported by nanofibrous membranes is different from that on the morphologies of conventional PA-TFC membranes supported by casting polysulfone (PSf) layer, which can be attributed to the different shrinkage between the casting PSf supporting layer and nanofibrous supporting membranes.

The hydrophilicity of the prepared PVDF-NCMs with different curing times, which is reflected by the contact angles, is shown in Fig. 10. Obviously, the curing time has an important effect on the contact angles

of the obtained membranes. The membranes with the curing times of 5 and 15 min have a lower initial contact angles than the membrane with curing time of 25 min, which is attributed to the rougher surface reflected in Fig. 9. Additionally, with increasing the contacting times the contact angles decrease more and more rapidly when the curing times are increased from 5 to 25 min. The decrease rate of the contact angles is supposed to be related with the density of the membranes. Therefore, it can be concluded that the density of the polyamide layer of the membranes gradually decreases as the curing time increases. The density of the polyamide layer is in close relation to the separation properties. Thus, the curing time will definitely influence the permeations and salt rejections of the membranes.

The separation properties reflected by the permeations and salt rejections of the obtained membranes with different curing times are shown in Fig. 11. Obviously, the curing times of the membranes can significantly influence the separation properties. With increasing curing times from 5 to 15 min and then to 25 min, the permeations increase from 14.8 to 16.5 L/m² h and then to 18.6 L/m² h. However, the salt rejections decrease from 96.5 to 94.4% and then to 90.1%. As discussed above, increasing the curing times can decrease the density of the separating polyamide layer of the membranes, which will increase the permeations but decrease the salt rejections. It should be noted that for the conventional PSf casting layer-supported polyamide TFC membranes, increasing curing temperatures or curing times will increase the salt rejections and decrease the permeations due to the compaction of the supporting layer [35]. However, for the PVDF-NCMs obtained here, the results are opposite. This difference can be attributed to the unique properties of the supporting nanofibrous membranes. The curing can induce the expansion of the nanofibers, which can increase the pores of the membranes and further decrease the density of the polyamide layer.

3.4. Discussion of the PVDF-NCMs with optimized conditions

The PVDF-NCMs obtained under the optimized conditions (MPD: 2.5 wt%, TMC: 0.125 wt%, curing time: 15 min) with the best separation properties is further analyzed to comprehensively evaluate the applicable properties of this kind of novel membrane.

AFM analysis is carried out to further investigate the surface morphologies of the obtained PVDF-NCMs with optimized conditions (Fig. 12). Three-dimensional

Table 1

Comparisons of the separation properties between the PA-based PVDF-NCMS obtained herein and the commercial/literature-reported PA-TFC RO membranes

Membranes	Feed NaCl concentrations (ppm)	Operation pressures (bar)	Permeations (L/m ² h bar)	Salt rejections
<i>Commercial PA-TFC RO membranes</i>				
Hydranatics LFC1 [37]	1,500	15.5	3.03	>99.5%
Hydranatics LFC3 [37]	1,500	15.5	2.58	>99.6%
Hydranatics SWC3 [15]	1,600	11.4	0.42	>96%
GE OSMO-MUNIRO [37]	2,000	15.5	2.90	>99.5%
GE DS-11 AG Series [37]	2,000	15.5	2.77	>99.5%
SHN (Korea) [38]	32,000	62.1	0.56	>99%
DOW FilmTech, BW30 [39]	32,000	55	0.74	>99%
DOW FilmTech, BW30LE [39]	2,000	10	3.72	>99%
DOW FilmTech, SW30LE [40]	2,000	18	0.86	>97%
<i>Literature reported PA-TFC RO membranes</i>				
Bao et al. [24]	2,000	16	1.19	>96%
Rana et al. [11]	32,000	55.2	0.75	>94%
Zhao et al. [41]	2,000	15.5	1.42	>98%
Hirose et al. [42]	1,500	15.0	2.8	>99.5%
Prakash Rao et al. [43]	2,000	17.2	3.49	95%
Kim et al. [44]	2,000	15.5	1.66	>96%
Yong et al. [45]	2,000	16.0	1.88	98%
Ghosh et al. [35]	2,000	17.2	1.51	>98%
Kong et al. [46]	2,000	15.0	0.63	>97%
Xie et al. [37]	2,000	15.5	2.65	>99%
Kwon et al. [36]	2,000	15.0	3.25	>98%
<i>The PA based PVDF-NCMS obtained herein</i>				
	2,000	8.0	2.06	>94%

10- μm scan images for the membranes are taken, and the root-mean-square roughness (R_{ms}) and peak-to-valley ($R_{\text{p-v}}$) distance of the membrane surface are calculated and the results are listed at the bottom table. The R_{ms} and $R_{\text{p-v}}$ of the PVDF-NCMS are, respectively, to be 193 and 768 nm. For the conventional PSf-supported polyamide TFC membranes, R_{ms} and $R_{\text{p-v}}$ are, respectively, to be ~ 100 nm and 300–400 nm [36]. Therefore, the membranes obtained here have rougher surface, which may be favorable for the hydrophilicity but disadvantageous for antifouling properties.

The cross-sectional SEM images of the PVDF-NCMS with optimized conditions are shown in Fig. 13. The average thicknesses of the nanofibrous supporting layer and separating polyamide layer are, respectively, to be ~ 18 μm and ~ 535 nm. The thicknesses of the PSf supporting layer and the polyamide layer for the conventional TFC membranes are ~ 40 μm and 100–200 nm [36]. The thinner supporting layer can be favorable for the permeations of the membranes. In addition, the high porosity of the nanofibrous membranes can further increase the permeations. The sepa-

rating polyamide layer is comparatively thicker. Principally, the thicker separation layer should supply a higher salt rejection. However, although with the higher thickness, the salt rejection of the obtained PVDF-NCMS is not higher, which is ascribed to the lower density.

The separation properties of the obtained PVDF-NCMS prepared under the optimized conditions are compared with that of the main commercial and other lab-scale literature-reported PA-TFC RO membranes as shown in Table 1. The salt rejections of the PVDF-NCMS are not as high as that of the compared both commercial and literature-reported PA-TFC RO membranes. The comparatively low salt rejection of PVDF-NCMS might be ascribed to the effect of nanofibrous mats of sublayers. High porous structure of electrospun sublayer can decrease the cross-linking of polyamide layer, which decreased the salt rejection. Although the permeation of the PVDF-NCMS is lower than most of the commercial ones, the advantage over the lab-scale literature reported ones is apparent. More importantly, the operating pressure of the

PVDF-NCMs is the lowest among all the membranes. Therefore, this kind of membrane is more energy-saving and cost-effective and can be used in some unique desalination areas which need as high as permeations and moderate salt rejections.

4. Conclusions

Summarily, novel PVDF-NCMs with promising desalination properties are fabricated by the interfacial polymerization on the chitosan-coated electrospun PVDF nanofibrous membranes. The effect of various factors on the morphologies and separation properties of the PVDF-NCMs, including MPD and TMC concentrations, and curing times, are systematically investigated. Under the optimized experimental conditions, the PVDF-NCMs show separation properties with a permeation of 16.5 L/m² h and salt rejection of 94.4%. Compared with the conventional PA-TFC membranes, the PVDF-NCMs have a rougher surface and a lower separation layer density. The PVDF-NCMs show apparent permeation advantages with comparatively lower salt rejections. More importantly, the operating pressure of this kind of membrane is only 8 bar, which is lower than most of the currently used and researched polyamide TFC membranes. Thus, they are more cost-effective and can be used in some unique desalination areas which need as high as permeations and moderate salt rejections. It is believed that with more work going on, this kind of membrane can be a promising candidate in securing the novel low-energy cost desalination technologies and membranes.

Acknowledgments

This study was supported by Marine Public Welfare Industry Special Funds: Island Multiple Integrated Water Supply Technology Research and Application Demonstration (201405035); Central-Level Research Institutes Fundamental Research Team Project: Research on Anti-scaling Technologies of High-pressure Seawater Desalination Membranes (K-JBYMF-2015-T02).

References

- [1] S.J. Kim, S.H. Ko, K.H. Kang, J. Han, Direct seawater desalination by ion concentration polarization, *Nat. Nanotechnol.* 5 (2010) 297–301.
- [2] G.R. Xu, J.N. Wang, C.J. Li, Strategies for improving the performance of the polyamide thin film composite (PA-TFC) reverse osmosis (RO) membranes: Surface modifications and nanoparticles incorporations, *Desalination* 328 (2013) 83–100.
- [3] N. Misdan, W. Lau, A. Ismail, Seawater reverse osmosis (SWRO) desalination by thin-film composite membrane-current development, challenges and future prospects, *Desalination* 287 (2012) 228–237.
- [4] D. Li, H. Wang, Recent developments in reverse osmosis desalination membranes, *J. Mater. Chem.* 20 (2010) 4551–4566.
- [5] H.B. Park, B.D. Freeman, Z.B. Zhang, M. Sankir, J.E. McGrath, Highly chlorine-tolerant polymers for desalination, *Angew. Chem. Int. Ed.* 47 (2008) 6019–6024.
- [6] L. He, D. Li, G. Zhang, P.A. Webley, D. Zhao, H. Wang, Synthesis of carbonaceous poly(furfuryl alcohol) membrane for water desalination, *Ind. Eng. Chem. Res.* 49 (2010) 4175–4180.
- [7] A. Sotto, A. Rashed, R.X. Zhang, A. Martínez, L. Braken, P. Luis, B. Van der Bruggen, Improved membrane structures for seawater desalination by studying the influence of sublayers, *Desalination* 287 (2012) 317–325.
- [8] V.T. Do, C.Y. Tang, M. Reinhard, J.O. Leckie, Degradation of polyamide nanofiltration and reverse osmosis membranes by hypochlorite, *Environ. Sci. Technol.* 46 (2012) 852–859.
- [9] V. Perez-Moreno, C.B. Bonilla-Suarez, M. Fortanell-Trejo, G. Pedraza-Aboytes, Seawater desalination using modified ceramic membranes, *Ind. Eng. Chem. Res.* 51 (2012) 5900–5904.
- [10] J. Xu, X. Feng, C. Gao, Surface modification of thin-film-composite polyamide membranes for improved reverse osmosis performance, *J. Membr. Sci.* 370 (2011) 116–123.
- [11] D. Rana, Y. Kim, T. Matsuura, H.A. Arafat, Development of antifouling thin-film-composite membranes for seawater desalination, *J. Membr. Sci.* 367 (2011) 110–118.
- [12] Z. Zhang, Z. Wang, J. Wang, S. Wang, Enhancing chlorine resistances and anti-biofouling properties of commercial aromatic polyamide reverse osmosis membranes by grafting 3-allyl-5, 5-dimethylhydantoin and N, N'-Methylenebis (acrylamide), *Desalination* 309 (2013) 187–196.
- [13] H. Karkhanechi, R. Takagi, H. Matsuyama, Biofouling resistance of reverse osmosis membrane modified with polydopamine, *Desalination* 336 (2014) 87–96.
- [14] A.M. Saenz de Jubera, J.H. Herbison, Y. Komaki, M.J. Plewa, J.S. Moore, D.G. Cahill, B.J. Mariñas, Development and performance characterization of a polyamide nanofiltration membrane modified with covalently bonded aramide dendrimers, *Environ. Sci. Technol.* 47 (2013) 8642–8649.
- [15] J.S. Louie, I. Pinnau, M. Reinhard, Effects of surface coating process conditions on the water permeation and salt rejection properties of composite polyamide reverse osmosis membranes, *J. Membr. Sci.* 367 (2011) 249–255.
- [16] P.R.D. Abhijit Sarkar, P.I. Carver, J.L. Rousseau, Surface modification of polyamide reverse osmosis membranes, US 20120024789A1, United States, 2012.
- [17] D. Saeki, T. Tanimoto, H. Matsuyama, Prevention of bacterial adhesion on polyamide reverse osmosis membranes via electrostatic interactions using a cationic phosphorylcholine polymer coating, *Colloids Surf. A* 443 (2014) 171–176.

- [18] Y. Zhang, C. Zhao, H. Yan, G. Pan, M. Guo, H. Na, Y. Liu, Highly chlorine-resistant multilayer reverse osmosis membranes based on sulfonated poly(arylene ether sulfone) and poly(vinyl alcohol), *Desalination* 336 (2014) 58–63.
- [19] Q. Cheng, Y. Zheng, S. Yu, H. Zhu, X. Peng, J. Liu, J. Liu, M. Liu, C. Gao, Surface modification of a commercial thin-film composite polyamide reverse osmosis membrane through graft polymerization of N-isopropylacrylamide followed by acrylic acid, *J. Membr. Sci.* 447 (2013) 236–245.
- [20] N. Ma, J. Wei, R. Liao, C.Y. Tang, Zeolite-polyamide thin film nanocomposite membranes: Towards enhanced performance for forward osmosis, *J. Membr. Sci.* 405–406 (2012) 149–157.
- [21] C. Kong, A. Koushima, T. Kamada, T. Shintani, M. Kanezashi, T. Yoshioka, T. Tsuru, Enhanced performance of inorganic-polyamide nanocomposite membranes prepared by metal-alkoxide-assisted interfacial polymerization, *J. Membr. Sci.* 366 (2011) 382–388.
- [22] M. Fathizadeh, A. Aroujalian, A. Raisi, Effect of added NaX nano-zeolite into polyamide as a top thin layer of membrane on water flux and salt rejection in a reverse osmosis process, *J. Membr. Sci.* 375 (2011) 88–95.
- [23] D. Li, L. He, D. Dong, M. Forsyth, H. Wang, Preparation of silicalite–polyamide composite membranes for desalination, *Asia-Pac. J. Chem. Eng.* 7 (2012) 434–441.
- [24] M. Bao, G. Zhu, L. Wang, M. Wang, C. Gao, Preparation of monodispersed spherical mesoporous nanosilica–polyamide thin film composite reverse osmosis membranes via interfacial polymerization, *Desalination* 309 (2013) 261–266.
- [25] H. Zhao, S. Qiu, L. Wu, L. Zhang, H. Chen, C. Gao, Improving the performance of polyamide reverse osmosis membrane by incorporation of modified multi-walled carbon nanotubes, *J. Membr. Sci.* 450 (2014) 249–256.
- [26] S. Kaur, S. Sundarrajan, D. Rana, T. Matsuura, S. Ramakrishna, Influence of electrospun fiber size on the separation efficiency of thin film nanofiltration composite membrane, *J. Membr. Sci.* 392–393 (2012) 101–111.
- [27] A.K. Ghosh, E.M.V. Hoek, J.M. Nygaard, Micro-and nanocomposite support structures for reverse osmosis thin film membranes, US 008029857B2, United States, 2011.
- [28] X. Wang, X. Chen, K. Yoon, D. Fang, B.S. Hsiao, B. Chu, High flux filtration medium based on nanofibrous substrate with hydrophilic nanocomposite coating, *Environ. Sci. Technol.* 39 (2005) 7684–7691.
- [29] R. Wang, Y. Liu, B. Li, B.S. Hsiao, B. Chu, Electrospun nanofibrous membranes for high flux microfiltration, *J. Membr. Sci.* 392–393 (2012) 167–174.
- [30] Z. Zhao, J. Zheng, M. Wang, H. Zhang, C.C. Han, High performance ultrafiltration membrane based on modified chitosan coating and electrospun nanofibrous PVDF scaffolds, *J. Membr. Sci.* 394–395 (2012) 209–217.
- [31] K. Yoon, B.S. Hsiao, B. Chu, High flux nanofiltration membranes based on interfacially polymerized polyamide barrier layer on polyacrylonitrile nanofibrous scaffolds, *J. Membr. Sci.* 326 (2009) 484–492.
- [32] S. Kaur, S. Sundarrajan, D. Rana, T. Matsuura, S. Ramakrishna, Influence of electrospun fiber size on the separation efficiency of thin film nanofiltration composite membrane, *J. Membr. Sci.* 392–393 (2012) 101–111.
- [33] G.R. Xu, J.N. Wang, C.J. Li, Polyamide nanofilm composite membranes (NCMs) supported by chitosan coated electrospun nanofibrous membranes: Preparation and separation performance research, *Desalination* 328 (2013) 31–41.
- [34] L. Huang, N.N. Bui, M.T. Meyering, T.J. Hamlin, J.R. McCutcheon, Novel hydrophilic nylon 6,6 microfiltration membrane supported thin film composite membranes for engineered osmosis, *J. Membr. Sci.* 437 (2013) 141–149.
- [35] A.K. Ghosh, B.H. Jeong, X. Huang, E.M.V. Hoek, Impacts of reaction and curing conditions on polyamide composite reverse osmosis membrane properties, *J. Membr. Sci.* 311 (2008) 34–45.
- [36] Y.N. Kwon, S. Hong, H. Choi, T. Tak, Surface modification of a polyamide reverse osmosis membrane for chlorine resistance improvement, *J. Membr. Sci.* 415–416 (2012) 192–198.
- [37] W. Xie, G.M. Geise, B.D. Freeman, H.S. Lee, G. Byun, J.E. McGrath, Polyamide interfacial composite membranes prepared from m-phenylene diamine, trimesoyl chloride and a new disulfonated diamine, *J. Membr. Sci.* 403–404 (2012) 152–161.
- [38] H. Choi, J. Park, T. Tak, Y.N. Kwon, Surface modification of seawater reverse osmosis (SWRO) membrane using methyl methacrylate-hydroxy poly(oxyethylene) methacrylate (MMA-HPOEM) comb-polymer and its performance, *Desalination* 291 (2012) 1–7.
- [39] C. Wang, G.K. Such, A. Widjaya, H. Lomas, G. Stevens, F. Caruso, S.E. Kentish, Click poly(ethylene glycol) multilayers on RO membranes: Fouling reduction and membrane characterization, *J. Membr. Sci.* 409–410 (2012) 9–15.
- [40] S. Azari, L. Zou, Using zwitterionic amino acid l-DOPA to modify the surface of thin film composite polyamide reverse osmosis membranes to increase their fouling resistance, *J. Membr. Sci.* 401–402 (2012) 68–75.
- [41] L. Zhao, P.C.Y. Chang, W.S.W. Ho, High-flux reverse osmosis membranes incorporated with hydrophilic additives for brackish water desalination, *Desalination* 308 (2013) 225–232.
- [42] M. Hirose, H. Ito, Y. Kamiyama, Effect of skin layer surface structures on the flux behaviour of RO membranes, *J. Membr. Sci.* 121 (1996) 209–215.
- [43] A. Prakash Rao, S.V. Joshi, J.J. Trivedi, C.V. Devmurari, V.J. Shah, Structure-performance correlation of polyamide thin film composite membranes: Effect of coating conditions on film formation, *J. Membr. Sci.* 211 (2003) 13–24.
- [44] S.H. Kim, S.Y. Kwak, T. Suzuki, Positron annihilation spectroscopic evidence to demonstrate the flux-enhancement mechanism in morphology-controlled thin-film-composite (TFC) membrane, *Environ. Sci. Technol.* 39 (2005) 1764–1770.
- [45] Z. Yong, Y. Sanchuan, L. Meihong, G. Congjie, Polyamide thin film composite membrane prepared from m-phenylenediamine and m-phenylenediamine-5-sulfonic acid, *J. Membr. Sci.* 270 (2006) 162–168.
- [46] C. Kong, M. Kanezashi, T. Yamamoto, T. Shintani, T. Tsuru, Controlled synthesis of high performance polyamide membrane with thin dense layer for water desalination, *J. Membr. Sci.* 362 (2010) 76–80.